Evidence for ferromagnetic instability in a repulsive Fermi gas of ultracold atoms

G. Valtolina[1,2,3], F. Scazza[1,2], A. Amico[1,2], A. Burchianti[1,2],
A. Recati[4,5], T. Enss[6], M. Inguscio[1,2], M. Zaccanti[1,2,*] & G. Roati[1,2]
[1]*INO-CNR, Via Nello Carrara 1, 50019 Sesto Fiorentino, Italy*
[2]*LENS and Università di Firenze, Via Nello Carrara 1, 50019 Sesto Fiorentino, Italy*
[3]*Scuola Normale Superiore, Piazza dei Cavalieri, 7, 56126 Pisa, Italy*
[4]*INO-CNR BEC Center and Dipartimento di Fisica, Università di Trento, 38123 Povo, Italy*
[5]*Technische Universität München, James-Franck-Straße 1, 85748 Garching, Germany and*
[6]*Universität Heidelberg, Philosophenweg 19, 69120 Heidelberg, Germany*

Ferromagnetism is among the most spectacular manifestations of interactions within many-body fermion systems[1]. In contrast to weak-coupling phenomena, it requires strong repulsion to develop, making a quantitative description of ferromagnetic materials notoriously difficult. This is especially true for itinerant ferromagnets[2–4], where magnetic moments are not localized into a crystal lattice. In particular, it is still debated whether the simplest case envisioned by Stoner[5] of a homogeneous Fermi gas with short-range repulsive interactions can exhibit ferromagnetism at all. In this work, we positively answer this question by studying a clean model system consisting of a binary spin-mixture of ultracold ^{6}Li atoms, whose repulsive interaction is tuned via a Feshbach resonance. We drastically limit detrimental pairing effects[6] that affected previous studies[7–9] by preparing the gas in a magnetic domain-wall configuration. We reveal the ferromagnetic instability by observing the softening of the spin-dipole collective mode that is unequivocally linked to the increase of the spin susceptibility while approaching the ferromagnetic transition for increasing interaction strength[10]. The ferromagnetic behaviour of the gas beyond the critical value of repulsion is additionally confirmed by the emergence of a time window during which the two spin domains remain immiscible, corresponding to a vanishing spin diffusion[11,12]. We extract the critical values of repulsion and temperature for a ferromagnetic phase to exist, at least in a metastable sense. Our findings provide a benchmark for current and future theories[2,13] supporting a minimal description of itinerant ferromagnetism, and our approach opens up new perspectives for investigating repulsive Fermi systems.

Stoner's model of ferromagnetism[5] represents a cornerstone for our understanding of a variety of systems which owe their magnetic properties to itinerant, i.e. delocalised, fermions, such as transition metals[1,2], normal ^{3}He liquids[14], neutron and quark matter within the crust of neutron stars[3,4]. Stoner's picture is an intuitively simple mean-field model: a free electron gas is predicted to become ferri- or ferromagnetic once a short-ranged screened Coulomb repulsion between oppositely oriented electron spins overcomes the effect of Fermi pressure, which would favour a paramagnetic state with no spin ordering. A sufficiently strong repulsion promotes the parallel alignment of magnetic moments, at the price of an increased kinetic energy, leading to spontaneous magnetization. Although Stoner's approach is quantitatively unreliable since it neglects significant beyond mean-field effects[1,2], more rigorous approaches based on Landau's Fermi liquid theory and quantum Monte Carlo (QMC) calculations[6,13,15–19] confirm the occurrence of a ferromagnetic instability driven just by short-range repulsion in a homogenous Fermi gas. Still, the ferromagnetic behaviour of such a minimal system lacks experimental evidence. Investigating this scenario with solid-state materials is complicated by the unavoidable presence of intricate band structures and disorder[2]. Liquid ^{3}He in its normal phase, although presenting a very high magnetic susceptibility, does not become ferromagnetic even at the highest applicable pressures, being the increase of susceptibility mainly ascribable to mass renormalisation[14].

Ultracold atomic Fermi gases appear in turn as an ideal environment for testing Stoner's model[15]. The harmonic confinement leads to simple dispersion relations and the short-range repulsive interactions between spin-$\uparrow$ and $\downarrow$ ultracold atoms, encoded in the s-wave scattering length a, can be continuously adjusted via magnetic Feshbach resonances[20]. Since the populations of $\uparrow$ and $\downarrow$ fermions are independently conserved, spontaneous magnetization translates into development of spatial domains with unequal $\uparrow$ and $\downarrow$ densities. However, first pioneering experiments aiming to observe the para-to-ferro-magnetic transition in ultracold atomic gases[7,8] found the Stoner instability to be hindered by the pairing one[6]. The latter arises from the fact that zero-range repulsion necessarily implies the existence of a weakly bound molecular state[20]. Hence, the repulsive Fermi gas corresponds to a metastable excited (upper) energy branch of the many-body problem[13,21,22] (see Fig. 1a), a fact that makes it intrinsically unstable against decay processes[8,9,22] that are rapid with respect to the development of magnetic domains[6,8,9]. In our experiment we are able to maintain a Fermi gas on the upper branch by preparing a spin $\uparrow - \downarrow$ mixture in an artificial magnetic domain-wall structure (see Fig. 1b). Such a fully-ferromagnetic initial configuration features a vanishingly small $\uparrow - \downarrow$ density overlap in contrast to a paramagnetic state[7,8]. This greatly suppresses the effect of pairing processes, ensuring that the overall relaxation rate remains much slower than the Fermi energy.

We reveal the ferromagnetic instability through two distinct but interconnected measurements of spin dynamics. On the one hand, by probing the spin-dipole mode[10], i.e. the out-of-

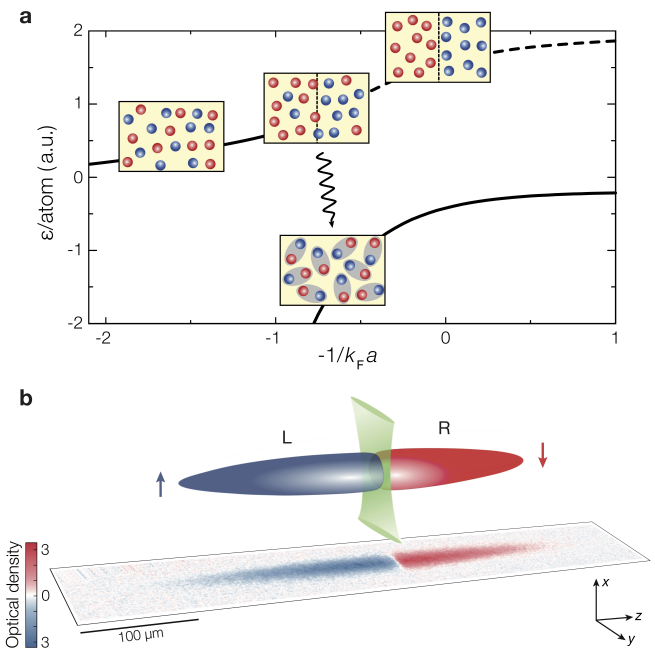

FIG. 1. **Realising an artificial ferromagnet with a repulsive Fermi gas of ultracold atoms. a,** A Fermi mixture with resonant short-range interactions, parametrised by $1/k_F a$, features two distinct energy branches, the lower (upper) being associated to a net inter-species attraction (repulsion). Ferromagnetism develops at strong repulsion along the upper branch, which becomes unstable due to enhanced decay processes onto the lower branch. Depending on the spin imbalance, the lower branch corresponds either to a paired phase or to an attractive Fermi liquid. **b,** In our experiment we circumvent the pairing instability by preparing an atomic Fermi gas in a ferromagnetic domain-wall structure, probed via spin-selective *in situ* imaging (see lower image). The initial state is obtained by segregating the two spin components into two initially disconnected reservoirs by means of a 2 μm thin optical barrier (sketched in green).

phase relative oscillation of the approaching spin $\uparrow - \downarrow$ clouds, we obtain information on the behaviour of the spin susceptibility as a function of interaction. On the other hand, studying spin diffusion[11,12] at short and long evolution times provides important insights on the stability of the ferromagnetic state and on its relaxation mechanisms, respectively. In particular, while it appears infeasible for a paramagnetic gas to become ferromagnetic due to short-range repulsion[6,8,13], our work shows that a ferromagnetic state, once artificially created, can exist in a metastable sense.

We initially prepare a weakly interacting mixture of ultracold ^{6}Li atoms[23], equally populating the two lowest Zeeman states, hereafter denoted as $|\uparrow\rangle$ and $|\downarrow\rangle$. The atoms are held in a cylindrical optical dipole trap with axial and radial frequencies $\nu_z \simeq 21$ Hz and $\nu_\perp \simeq 265$ Hz, respectively. By adjusting the evaporation procedure we can tune the degree of degeneracy from $T/T_F < 0.1$ up to ~ 1. Here T is the gas temperature, while T_F is the Fermi temperature of a single-component Fermi gas of N atoms in a harmonic trap, given by $k_B T_F = E_F = h(6N\nu_z\nu_\perp^2)^{1/3}$, with h and k_B denoting the Planck's and Boltzmann's constants. At a magnetic field of about 1 G, where the magnetic moments of $|\uparrow\rangle$ and $|\downarrow\rangle$ states are opposite, the application of a magnetic field gradient allows us to spatially separate the two spin components along the weak axis of the trap. Once the overlap between the two clouds is perfectly zero, we superimpose a 2 μm thin optical repulsive barrier as high as $V_0 \sim 10 E_F$ onto the centre of the harmonic potential, in order to split the trap into two independent reservoirs[24], as sketched in Fig. 1b. We then adiabatically turn off the magnetic field gradient and end up with all $\uparrow$ ($\downarrow$) fermions in the left (right) reservoir (see also Methods and Supplementary Information). This creates two macroscopic spin domains at rest, separated by a distance only a few times wider than the mean interparticle spacing of the gas. Such configuration resembles the density distribution expected for a spin-mixture undergoing full magnetization in an elongated harmonic trap, with a central domain wall of thickness around the interparticle spacing, additionally surrounded by an unpolarised low-density shell on the cloud surface.

From here, we let the two spin components start interacting by removing the optical barrier. Before switching off the barrier, the interaction strength is adjusted by setting the magnetic field close to the centre of a broad $\uparrow - \downarrow$ Feshbach resonance located around 832 Gauss[25].

In a first experiment the spin dynamics is triggered by abruptly switching off the barrier from its initial value $V_0 \simeq 10\, E_F$ on a μs timescale. Owing to the small initial separation of about 5 μm, the two spin clouds approach each other with small relative momentum $\hbar k \ll \hbar k_F = \sqrt{2 m_{Li} E_F}$. We follow the clouds dynamics by resonant *in-situ* absorption imaging (see Methods), monitoring the evolution of the two spin domains. On top of an overall slow drift, the relative distance between their centres of mass $d(t) = z_\uparrow(t) - z_\downarrow(t)$ presents a small-amplitude out-of-phase oscillation, signalling the excitation of the spin-dipole mode (see Fig. 2a-c). The measurement of the spin-dipole frequency ν_{SD}, analogously to the one of spin fluctuations[8,10], is a prominent tool for disclosing the magnetic behaviour of the system: the trend of ν_{SD} is directly related to the inverse of the spin susceptibility χ, weighted over the inhomogeneous density distribution[10] (see Methods).

In particular, the increase of χ and its divergence at the ferromagnetic transition[10,18], first reached in the denser central region of the trap, are univocally identified by a substantial decrease of ν_{SD}, i.e. by a softening of the spin-dipole mode.

The measurement of this collective oscillation is extremely challenging when starting from a paramagnetic configuration due to strong damping[26] and inelastic processes[8,22]. Here, in turn, where the two spin domains just partially overlap over the timescale of the measurement, we are able to trace a few oscillation periods of the spin-dipole mode from which we extract ν_{SD} through a fit to a damped sinusoidal function (see Methods). Performing such a measurement at several magnetic field values, we obtain the trend of the spin-dipole frequency as a function of the repulsive interaction strength, displayed in Fig. 2d for two distinct temperatures. The interaction strength is described by the dimensionless parameter $\kappa_F a$, where κ_F (and correspondingly ϵ_F) is the average Fermi wave number (energy) weighted over the initial den-

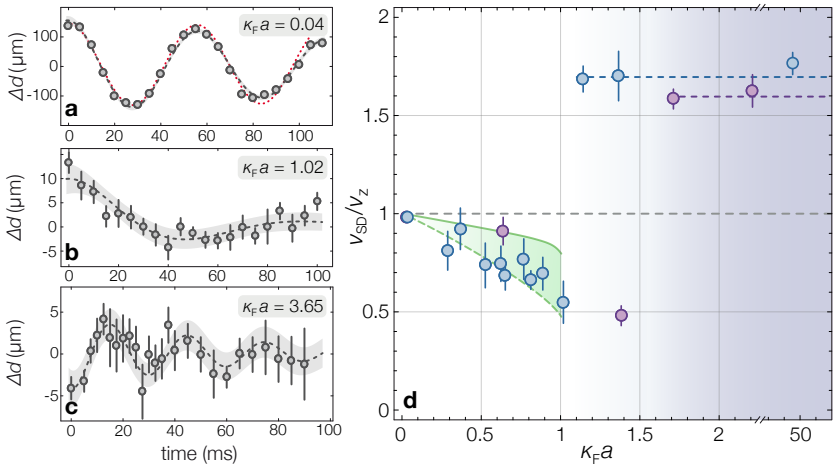

FIG. 2. **Spin-dipole mode of a repulsive Fermi gas across the ferromagnetic instability. a-c,** After subtracting a slow exponential drift from $d(t)$, the residual out-of-phase dynamics $\Delta d(t)$ of the two spin clouds after sudden barrier removal is fitted to a damped sinusoidal function (dashed lines), from which ν_{SD} is extracted for several interaction strengths. The bare trap oscillation is shown for comparison (dotted red line in **a**). Shaded areas denote the standard confidence bands of the fits. Data points result from at least 5 independent measurements with error bars given by the standard error of the mean (s.e.m.) combined with the uncertainty on the subtracted exponential drift. **d,** The normalised spin-dipole frequency ν_{SD}/ν_z is plotted versus $\kappa_F a$ for $T/T_F = 0.12(2)$ (blue circles) and $T/T_F = 0.25(4)$ (purple circles), with error bars being 95% confidence intervals of sinusoidal fits. A decrease of ν_{SD} followed by a clear discontinuity is visible, marking the critical interaction strength of the ferromagnetic instability. The dashed blue (violet) lines are the average ν_{SD}/ν_z measured beyond the critical point at $T/T_F = 0.12$ ($T/T_F = 0.25$) up to unitarity. The solid (dashed) green lines are the $T = 0$ predictions from a sum-rule approach assuming 25% (100%) $\uparrow - \downarrow$ spatial overlap (see Methods).

sity distribution close to the interface between the two domains (see Methods). Let us discuss here the results for the colder samples at $T/T_F \sim 0.12(2)$. By starting from the weakly interacting regime, where $\nu_{SD} \simeq \nu_z$ (see Fig. 2a), an increase of the interspecies repulsion leads to a progressive reduction of the spin-dipole frequency, down to values as low as $\nu_{SD} \simeq 0.6\,\nu_z$ at about $\kappa_F a \simeq 1$ (Fig. 2b). We find the decrease of ν_{SD} to be accompanied by a strong increase of the damping of the oscillations[26]. By further increasing the interspecies repulsion, an abrupt change occurs in the spin dynamics: for $\kappa_F a \gtrsim 1.1$, the spin-dipole frequency jumps above the bare trap frequency, $\nu_{SD} \simeq 1.70(4)\nu_z$ (see Fig. 2c), while the damping of the oscillations is strongly reduced. Once this narrow interaction region is crossed, a further increase of $\kappa_F a$ does not produce any significant change, neither in the damping rate nor in ν_{SD}. Our observation of the mode softening matches a recent linear-response theory prediction[10] (see lines in Fig. 2d) based on a sum-rule approach and on the knowledge of $\chi(\kappa_F a)$ obtained by QMC calculations for a homogeneous zero-temperature Fermi gas[18] (see Methods). The good agreement between such a non-perturbative theory approach and the experimental data strongly suggests that the repulsive Fermi liquid exhibits the ferromagnetic instability at $\kappa_F a \simeq 1$. Furthermore, for $\kappa_F a > 1.1$, the value of ν_{SD} is in good agreement with theory models[27] based on the hydrodynamics of two repulsive spin clouds bouncing off each other and previous measurements at unitarity[11].

If the ferromagnetic phase were indefinitely stable above a critical $\kappa_F a$, the two spin domains would remain immiscible, i.e. spin diffusion would be impeded[26]. To investigate this aspect, we study spin diffusion in a second set of measurements, exploring various interaction and temperature regimes.

We initialise the dynamics by adiabatically lowering the barrier height through a 30 ms linear ramp from $V_0 \sim 10\,E_F$ down to $2\,E_F$, letting the two clouds slowly approach each other. Their relative distance is reduced from about 5 μm down to 1 μm, yet each spin domain remains confined within its own reservoir. At this point, we remove the barrier in 5 ms and we monitor the subsequent evolution of the relative population of the $i = \uparrow, \downarrow$ component in the left and right reservoirs, $M_i = (N_{i,L} - N_{i,R})/(N_{i,L} + N_{i,R})$, from which we obtain the magnetization $\Delta M = (M_\uparrow - M_\downarrow)/2$. Since the distance between the two nearby cloud edges is approximately equal to the local interparticle spacing at the interface between the two spin domains, this procedure does not excite any detectable relative centre-of-mass oscillation.

In Fig. 3a we show the short-time evolution $\Delta M(t)$ for different interaction strengths: above a critical value of repulsion, after an initial slight decrease of ΔM, we indeed observe a time window during which spin diffusion is completely arrested. The duration of this "plateau" in the spin dynamics is however finite, since the stability of our ferromagnetic state is limited by the intrinsic tendency of the system to relax from the excited upper branch onto lower-lying energy states[6,13] (see Fig. 1a). A thorough characterisation of this interesting feature is summarized in Fig. 3b, where we plot the measured plateau duration τ_p of constant ΔM as a function of $1/(\kappa_F a)$, for various temperatures. The value of τ_p is determined through a piecewise linear fit to the data, yielding zero when no noticeable halt of spin dynamics is detected. Our measurements provide several relevant informations. First, a non-zero τ_p is detected only above a critical $\kappa_F a$ value and

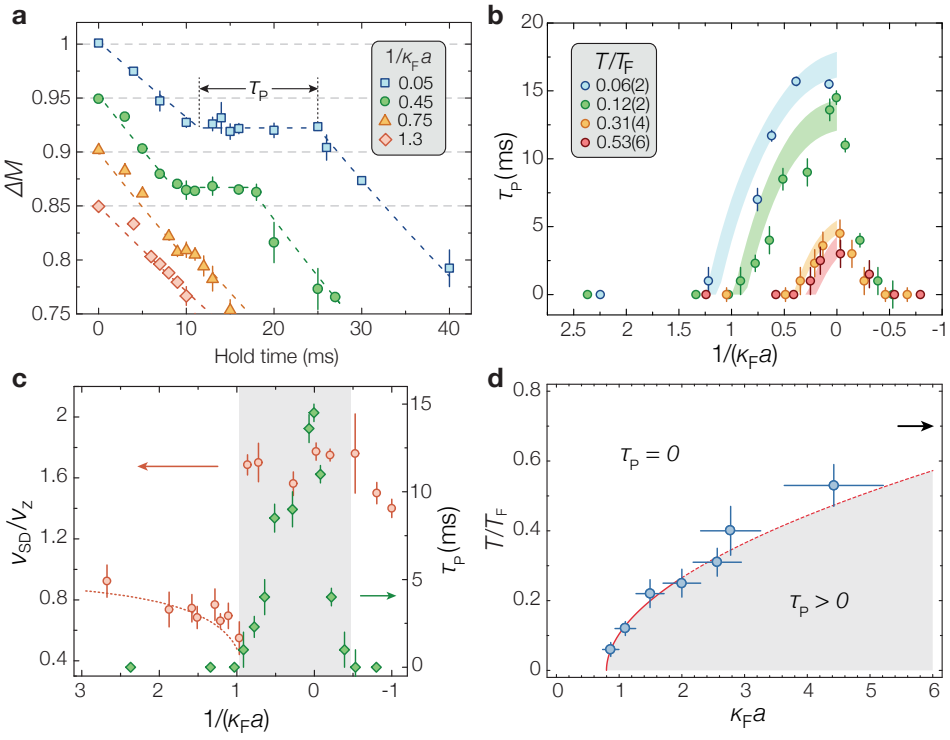

FIG. 3. **Metastability of an ultracold atomic ferromagnet. a,** Evolution of $\Delta M(t)$ for different interactions at $T/T_F = 0.12(2)$. For $\kappa_F a \geq 1.1$ a time window τ_p of vanishing spin diffusion is detected. Error bars are the s.e.m. of 4-5 independent measurements. Data sets are relatively shifted by 0.05 along the y-axis for clarity. **b,** τ_p from piecewise fits to the data (dashed lines in **a**) is plotted at varying $1/\kappa_F a$ for various temperatures, with error bars being the fit standard uncertainty. Shaded curves are derived from the proposed model for domain-wall melting (see Methods), adjusting E_{+c} within a 20% variation. **c,** Connection between τ_p (green diamonds) and ν_{SD} (red circles) at $T/T_F = 0.12(2)$. The dotted line represents the prediction on ν_{SD} for the repulsive Fermi liquid (see Fig 2d). **d,** (Meta-)stability ($\tau_p > 0$) region of the ferromagnetic state in the temperature-interaction plane. y-error bars denote the experimental uncertainty on T/T_F, while x-error bars account for the uncertainty on estimating the critical $\kappa_F a$ at which a $\tau_p > 0$ is observed. The solid line is a power-law fit (see text) to $T/T_F < 0.3$ points, extended over all values of $\kappa_F a$ as a dashed line. The black arrow marks the temperature at which $\tau_p = 0$ for any $\kappa_F a$.

below a certain T/T_F.

Notably, finite plateaus appear above an interaction strength nearly coincident with the one at which the spin-dipole mode frequency in Fig. 2d exhibits an abrupt change (see Fig. 3c). Furthermore, by increasing $\kappa_F a$ (increasing T/T_F) τ_p gets longer (shorter), reaching its maximum at the unitary point $1/(\kappa_F a) = 0$. On the other hand, no plateau in the dynamics is observed for $T/T_F \geq 0.7$. In addition, at low temperatures the trends for τ_p and ν_{SD} (see Fig. 3c) suggest that we access the upper branch even within a $1/(\kappa_F a) < 0$ narrow region beyond unitarity (see Supplementary Information).

We find the behaviour of the plateau duration for $1/(\kappa_F a) > 0$ to be captured (see curves in Fig. 3b) by a phenomenological model based only on the knowledge of the lifetime and energy spectrum of the upper and lower branches of the many-body system[28], calculated in the extremely polarised limit of one single $\uparrow$ ($\downarrow$) impurity embedded in a $\downarrow$ ($\uparrow$) Fermi gas[13,28]. Based on such a description, the ferromagnetic state is destroyed by inelastic processes occurring at the interface between the two macroscopic spin domains: fermions of one kind, overcoming the surface tension associated with a domain wall, can deposit an overall excess energy through decay from the upper to the lower branch. Only after some time, once a sufficient energy has been released into the system, the domain wall is melted and spin diffusion is established (see Methods).

In light of the close correspondence between the trends of ν_{SD} and τ_p (see Fig. 3c), we identify, for each temperature considered, the lowest $\kappa_F a$ value at which a non-zero τ_p is observed as the critical point beyond which a ferromagnetic phase would indefinitely exist in the absence of decay. This allows us to trace a curve in the interaction-temperature plane along which the repulsive Fermi liquid exhibits the ferromagnetic instability. The result of such analysis is presented in Fig. 3d. By fitting the $T/T_F < 0.3$ data points to $T/T_F \propto ((\kappa_F a)(T) - (\kappa_F a)(0))^{\alpha}$, we obtain $\alpha = 0.52(5)$ and $(\kappa_F a)(0) = 0.80(9)$. The fitted exponent matches within its uncertainty the value $\alpha = 1/2$ expected from the low-temperature behaviour of a Landau-Fermi liquid (see Supplementary Information). Furthermore, the extracted critical value $(\kappa_F a)(0)$ is found in good agreement with the ones obtained from recent QMC calculations[18,19].

Once spin diffusion is established, the analysis of the long-time evolution $\Delta M(t)$ (or equivalently $d(t)$) within a simple kinetic model (see Methods) allows us to determine also the spin drag coefficient[11] Γ_S as a function of temperature and

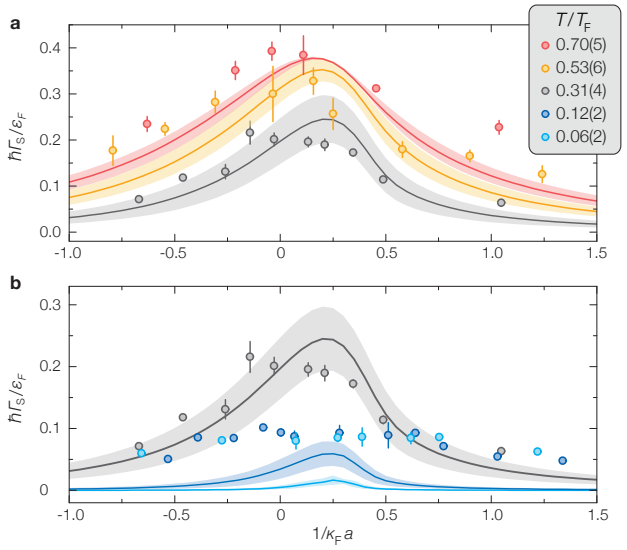

FIG. 4. **Spin drag coefficient of a resonant Fermi gas.** $\hbar\Gamma_S/\epsilon_F$ is plotted as a function of $1/\kappa_F a$ for **a,** $0.31 \leq T/T_F \leq 0.7$ and **b,** $T/T_F \leq 0.31$. Experimental points are obtained by fitting the dynamics at $t > 50$ ms to the solution of a diffusion model (see Methods). Error bars combine uncertainties of the fit and of our determination of ϵ_F. Lines are predictions from a T-matrix kinetic theory (see Supplementary Information), assuming the nominal initial T/T_F and allowing a $\pm 20\%$ temperature variation (shaded areas).

interaction.

The results are displayed in Fig. 4. These are compared with theoretical predictions for Γ_S, calculated for a single impurity moving in a homogeneous ideal Fermi gas within kinetic theory and T-matrix approximation for the scattering cross section (see Supplementary Information). The comparison is surprisingly good (see Fig. 4): the model is able to quantitatively reproduce not only the maximum Γ_S measured for $T/T_F \geq 0.3$, but also the overall trend versus $\kappa_F a$ at all temperatures. At low temperatures, although a poorer agreement with theory is expected as the T-matrix approximation is not quantitatively correct, the data sets exhibit an appreciable asymmetry around the unitary point towards $\kappa_F a > 0$. Such a feature, which disappears progressively as temperature is increased, highlights the significant effect of collisions within the medium of surrounding particles on the dynamical properties of the diffusing quasi-particles (see Supplementary Information). A similar asymmetry in transport coefficients has already been reported for the shear viscosity[29] and transverse spin diffusion[30], but not in previous measurements of the longitudinal spin diffusion[11].

In conclusion, we have probed the ferromagnetic behaviour of the repulsive Fermi gas by investigating a resonantly interacting ultracold ^{6}Li spin mixture.

Our study points to the occurrence of the ferromagnetic instability driven by short-range repulsive interactions, as first proposed by Stoner[5], and it provides a test-bed for theories on repulsive Fermi systems. In the future, our setup may be exploited to tackle other fundamental issues, such as identifying the order of the ferromagnetic transition[2], eventually in the presence of weak optical lattices[31], controlled disorder or reduced dimensionality.

METHODS

Experimental protocols

Our procedure to create weakly-interacting two-component Fermi mixtures of ^{6}Li atoms has been already described elsewhere[23] (see also Supplementary Information). The gas degeneracy parameter T/T_F is adjusted by exploiting the tunability of the collisional properties of ^{6}Li mixtures[25] during evaporation. We typically end up with 50×10^3 atoms per spin component, confined in a cigar-shaped harmonic potential characterised by axial (radial) trap frequency of $\nu_z = 21.0(1)$ Hz ($\nu_\perp = 265(5)$ Hz). To spatially separate the two spin components, at a magnetic field of about 1 G, where the $\uparrow$ and $\downarrow$ states possess equal but opposite magnetic moments, we turn on a magnetic quadrupole gradient of about 1 G/cm along the weak trap axis, that pushes the two spin clouds towards opposite directions. Once the overlap between the two components is zero, a repulsive optical potential centred at $z = 0$, and characterised by a short (long) $1/e^2$ waist of $w_z = 2.0(2)$ μm ($w_y = 840(30)$ μm) is employed to confine the two clouds into two disconnected reservoirs[24]. These are characterised by an axial oscillation frequency $\nu_R = 1.78(5)\nu_z$, and no appreciable particle tunnelling is detected over more than 2 seconds with a barrier height of about 10 E_F.

To excite the spin-dipole mode at a fixed Feshbach field, we abruptly switch off the barrier potential within less than one μs. The two spin clouds, initially separated by a distance of about 5 μm, start moving one towards the other at a small, though non-zero, relative velocity. From here on, we monitor the dynamics of the relative distance between the centres of mass of the two components. For each value of evolution time, in two independent and successive experimental runs, we acquire two *in-situ* absorption images with two high-intensity optical pulses, each of which is resonant only with one spin state. For each point of interaction, temperature, and evolution time herein investigated, the relative distance between the two clouds is determined by averaging over at least five independent measurements.

The centre of mass of each cloud is equivalently determined either via a Gaussian fit to the imaged density distribution (used for data displayed in Fig. 2a-c) or via the evaluation of the centre of mass z_i of each sample $i = \uparrow, \downarrow$ obtained via direct integration of the bare images. Once the spin dynamics is recorded, we fit $d(t) = (z_\uparrow - z_\downarrow)(t)$ to an exponential decay. By subtracting the fitted exponential drift from $d(t)$, we extract the spin-dipole collective dynamics $\Delta d(t)$, whose frequency is then derived by means of a damped sinusoidal function. Similarly, direct integration of the images at each evolution time allows to determine the relative population of the $i = \uparrow, \downarrow$ component in the left and right reservoirs, $M_i = (N_{i,L} - N_{i,R})/(N_{i,L} + N_{i,R})$, from which we obtain the magnetization $\Delta M = (M_\uparrow - M_\downarrow)/2$. The behaviour of $d(t)$ closely reflects the one of $\Delta M(t)$.

Effective Fermi energy and wavevector

In the main text we have defined κ_F and ϵ_F as relevant length and energy scales. These are evaluated by approximating the thin barrier at $z = 0$ as a delta-like potential. This is reasonable considering that the barrier thickness of $2\,\mu$m is about 70 times smaller than the typical Thomas-Fermi radius of the cloud along the z-axis. Namely, we approximate the density distribution of a Fermi gas of N atoms confined in a "half" of the harmonic trap bisected by the thin barrier as half of the distribution of a Fermi gas of $2N$ atoms in the whole harmonic trap. The latter is evaluated using the finite-temperature Fermi-Dirac distribution of an ideal Fermi gas $n_F(\mathbf{r}, T/T_F)$, given the measured T/T_F, trap frequencies and atom number. From $n_F(\mathbf{r}, T/T_F)$ the local wavevector and Fermi energy are given by $k_F(\mathbf{r}, T/T_F) = (6\pi^2 n_F(\mathbf{r}, T/T_F))^{1/3}$ and $E_F(\mathbf{r}, T/T_F) = \hbar^2 k_F^2(\mathbf{r}, T/T_F)/(2m_{\mathrm{Li}})$, respectively. The two parameters κ_F and ϵ_F are derived by averaging $k_F(\mathbf{r}, T/T_F)$ and $E_F(\mathbf{r}, T/T_F)$ over a region as thick as the local interparticle spacing $(6\pi^2)^{1/3}/k_F(x, y, 0, T/T_F)$ around $z = 0$. Parallel to this, integration of $n_F(\mathbf{r}, T/T_F)$ within such region yields the total number N_{int} of $\uparrow$ and $\downarrow$ fermions at the interface between the two spin domains (see Supplementary Information for details).

Sum-rule approach for the spin-dipole mode frequency

Given a perturbation operator D, the moments of the strength distribution function, or sum rules, are given by $m_k = \sum_n |\langle 0|D|n\rangle|^2 (E_n - E_0)^k$. In particular, the spin-dipole mode is excited by the operator $D = \sum_{i\uparrow} z_i - \sum_{i\downarrow} z_i$, where z is the longitudinal coordinate and $i_{\uparrow,\downarrow} = 1, \ldots, N_{\uparrow,\downarrow}$. The frequency ω_{SD} of the spin-dipole oscillation is estimated using the ratio (see Supplementary Information and Ref. 10):

$$\hbar^2 \omega_{SD}^2 = \frac{m_1}{m_{-1}} \tag{1}$$

Within the local density approximation (LDA) one can obtain (see Supplementary Information):

$$\omega_{SD}^2 = \frac{N_\uparrow + N_\downarrow}{m \int d\mathbf{r} z^2 \chi(n)} \tag{2}$$

where $\chi(n)$ is the zero-temperature magnetic susceptibility of a uniform gas obtained at the density n from QMC calculations[18]. The dashed green line plotted in Fig. 2 is calculated through Eq. (2) by inserting the density profile $n(r)$ of two fully overlapped spin components, determined in LDA using the equilibrium condition $\mu(n) - V_{\mathrm{trap}} = \mu_0$, where $\mu(n)$ is the chemical potential as a function of local density n from QMC calculations and μ_0 is fixed by the normalisation condition. The solid green line in Fig. 2 accounts instead for a reduced overlap of 25% around the trap centre, in closer analogy to the experimental condition. In this case, the integral in Eq. (2) over the outer spin-polarised regions contributes thus only with the spin susceptibility χ_0 of an ideal Fermi gas, yielding a reduced deviation of the spin-dipole frequency from the bare trap frequency. Therefore, we expect the measured frequencies to be higher than the results of Ref. 10, derived at full overlap. Consequently, the solid and dashed lines in Fig. 2 delimit a confidence region in which most experimental data are found. Most importantly, the critical interaction strength at which the abrupt change in ω_{SD} occurs does not depend on the initial overlap configuration. Moreover, the spin diffusion dynamics happens on a longer timescale ($\gtrsim 200\,$ms), as displayed in the Supplementary Information, compared to the spin-dipole period ($\sim 50 - 100\,$ms). Hence, while we cannot assume that the system oscillates near an equilibrium configuration as in linear-response theory, the (slow) timescale for diffusion is sufficiently separated from the (faster) timescale for the spin oscillations.

Polaron model for the domain-wall melting

The proposed explanation of the plateau data shown in Fig. 3 proceeds along the following line of thought. In the case of purely repulsive interaction, the ferromagnetic state, if energetically allowed, would be indefinitely stable and the miscibility of the two components would be prevented by the existence of a domain wall. In particular, a $\downarrow$ fermion at the interface would need to pay a finite amount of energy $\sigma > 0$ in order to access the other spin domain forming a repulsive polaron at energy E_+. In our metastable system, however, if a repulsive polaron is created, it can subsequently decay onto the lower branch with a rate Γ, releasing an energy equal to the mismatch between the two branches, $E_+ - E_-$. Hence, this two-step process will cause a net increase of energy $\Delta E = E_+ - E_- - \sigma$ at a rate Γ. Importantly, the behaviour of Γ, E_+ and E_- as a function of the interaction strength can be derived from recent non-perturbative theory approaches[13,28]. We assume that at the beginning of the dynamics, the energy associated to the domain wall is given by σN_{int}, N_{int} being the total number of fermions within a slice around $z = 0$ of total thickness equal to one interparticle spacing. The duration of the plateau τ_p is then set by the condition:

$$\sigma N_{int} = (E_+ - E_- - \sigma)\tau_p \Gamma \tag{3}$$

We assume that $\sigma = E_+ - E_{+c}$, where E_+ is the energy of a repulsive polaron, while E_{+c} is the energy of one free fermion at the interface, left as a phenomenological parameter, and is independently adjusted for each T/T_F herein investigated. From Eq. (23) we fit the experimental data by optimising the only free parameter E_{+c} (see also Supplementary Information).

Diffusion model for extracting the spin drag coefficient

The equation for the dynamics of the relative centre of mass $d = z_\uparrow - z_\downarrow$ can be easily obtained from the Boltzmann equation and is written as (see Supplementary Information)

$$\ddot{d} + \Gamma_s \dot{d} + \omega_z^2 d = 0, \tag{4}$$

where ω_z is the longitudinal trap frequncy, and Γ_s the spin drag coefficient due to collisions[11,12]. We obtain the experimental spin drag coefficient by fitting the solution of Eq. (4) to the data, considering as initial condition $d(0) = d_0$ and $\dot{d}(0) = 0$. The results are reported in Fig. 4.

In the same figure we compare the experimental results with a theoretical prediction based on a T-matrix approximation for the scattering cross-section corrected by the available scattering states in order to have a well defined scattering amplitude in the collisional integral.

The agreement is especially good down to temperatures as low as $T = 0.3\,T_F$. At lower temperatures, both the shape and the magnitude of the spin drag coefficient as a function of the interaction compare more poorly. This is expected since at very low temperature the Boltzmann approach is not quantitatively correct, and moreover the gas may suffer some heating during the dynamics due to decay processes, making its temperature higher than the one measured at the start of the dynamics, which is used for the comparison with the theory model. Further details are available in the Supplementary Information.

Acknowledgments. We thank A. Morales and J. Seman for contributions in the early stage of the experiment, and G. M. Bruun, C. Di Castro, C. Fort, S. Giorgini, P. Massignan, S. Pilati, R. Schmidt, W. Zwerger and the LENS Quantum Gases group for many stimulating discussions. This work was supported under European Research Council grants no. 307032 QuFerm2D, and no. 637738 PoLiChroM. A.R. acknowledges support from the Alexander von Humboldt foundation. T.E. acknowledges the Physics Department, Sapienza University Rome, for hospitality, and the Humboldt foundation for financial support during part of this work.

Competing Interests. The authors declare that they have no competing financial interests.

Author contributions

G.V., F.S., A.A., A.B., M.I., M.Z. and G.R. carried out the experimental work and A.R. and T. E. carried out the theoretical work.

Correspondence. Correspondence and requests for materials should be addressed to M.Z. (email: matteo.zaccanti@ino.it).

SUPPLEMENTARY INFORMATION

I. EXPERIMENTAL PROCEDURES

Our procedure to create weakly-interacting two-component Fermi mixtures of ^{6}Li atoms has been already described elsewhere[23]. To realize highly degenerate samples at $T/T_F \leq 0.2$, a balanced mixture of atoms equally populating the lowest and third-to-lowest Zeeman states (hereafter denoted $|1\rangle$ and $|3\rangle$, see Fig. 5a) is evaporated in a crossed optical dipole trap (ODT) at a bias magnetic field of 300 Gauss. At such a field the $|1\rangle - |3\rangle$ mixture features a large[25], though off-resonant, scattering length value of about -900 a_0 which makes the forced evaporation process extremely efficient[23]. Here a_0 is the Bohr's radius. We typically end up with $N \simeq 50 \times 10^3$ atoms per spin component, confined in a cigar-shaped harmonic potential characterized by axial and radial trap frequencies $\nu_z = 21.0(1)$ Hz and $\nu_\perp = 265(5)$ Hz, respectively. For the investigation of less degenerate samples, we either heat up in a controlled way the cloud by quickly turning off and on the ODT for an excitation time up to 1 ms, or we perform evaporation at 300 Gauss with a $|1\rangle - |2\rangle$ mixture. This features an interspecies scattering length of about -300 a_0, which makes the evaporation process less efficient than for the $|1\rangle - |3\rangle$ spin combination, leading to similar atom number and trap frequencies, though at higher temperature. The degeneracy parameter T/T_F is determined by fitting the cloud density profiles *in situ* or after 5 ms of time of flight to a finite temperature Fermi-Dirac distribution. At the end of evaporation in the $|1\rangle - |3\rangle$ mixture, we transfer all atoms from the $|3\rangle$ to the $|2\rangle$ state via a resonant 80 μs radio-frequency (RF) π-pulse. To avoid detrimental finite-state interaction effects, that would limit the transfer efficiency, we perform the transfer at a bias field of 584.5 G, where the scattering lengths of the $|1\rangle - |3\rangle$ and $|1\rangle - |2\rangle$ spin mixtures are equal and non-resonant[25].

Spin separation procedure

The procedure for creating two separate spin domains is here described and summarised in Fig. 5c. In order to spatially separate the $|1\rangle$ and $|2\rangle$ components, we adiabatically lower the magnetic field down to ~ 1 G, where the two states are essentially non-interacting and possess equal but opposite magnetic moments (see Fig. 5b). Subsequently, we turn on a magnetic quadrupole gradient of about 1 G/cm along the weak trap axis through a 40 ms linear ramp, shifting the two spin clouds in opposite directions. After 180 ms, once the overlap between the two components is completely zeroed, we turn on through a 40 ms linear ramp a strongly anisotropic 532 nm optical beam[24] centred at $z = 0$, and characterised by a short (long) $1/e^2$ waist of w_z =2.0(2) μm (w_x =840(30) μm). The beam, blue-detuned with respect to the 671 nm lithium main transition, results in a repulsive potential which bisects the cloud along the weak axis into two reservoirs. The typical maximum barrier height after the 40 ms ramp, is about 10 E_F, a value that impedes any appreciable particle tunnelling between the two reservoirs over more than 2 seconds. Once the two spin clouds are separated and disconnected, we adiabatically turn off the magnetic gradient and increase the bias Feshbach field with a 500 ms linear ramp up to the target value. To prevent atom losses due to the magnetic field gradient, after the evaporation we turn on two additional elliptic plug beams at 532 nm with short (long) waist of w_z =50 μm (w_y =120 μm). The short waist is aligned along the weak trap axis and the plugs enter perpendicularly to this, creating two effective repulsive walls that reduce as much as possible spilling of atoms due to the magnetic gradient. The plugs are turned on through a 200 ms linear ramp after evaporation and switched off through a 450 ms linear ramp when the Feshbach field is increased up to the final target value. The overall spin-separation procedure causes a decrease of about 25% of the atom population, whereas no change of T/T_F is measured. The degeneracy pa-

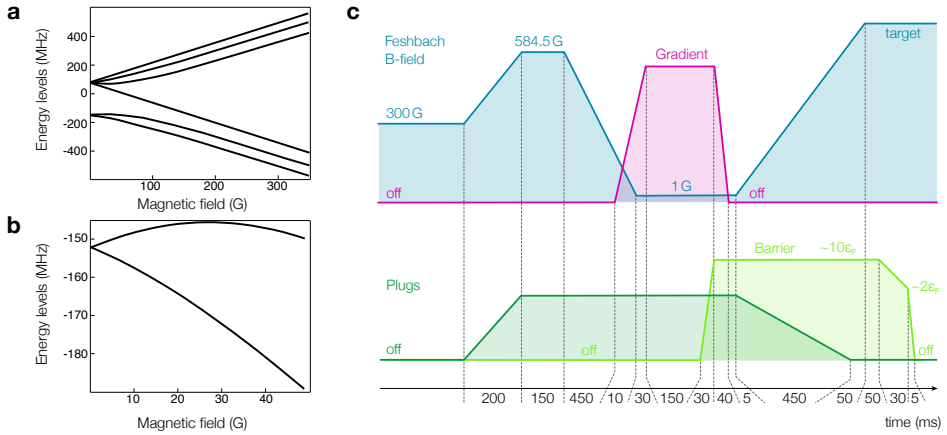

FIG. 5. (a) Hyperfine and Zeeman levels structure of ^{6}Li in the $F = 1/2$ and $F = 3/2$ manifolds as a function of the magnetic field. (b) Energy dependence of the two lowest Zeeman states ($|1\rangle$ and $|2\rangle$) at low magnetic field. Below 5 G, the two states have magnetic moments with nearly equal amplitude but opposite sign. (c) The experimental sequence used for spin separation is sketched: the Feshbach field (light blue), the magnetic gradient (purple), the side plugs (dark green) and the central barrier (light green) are plotted as a function of time.

rameter after spin separation is estimated by a finite temperature Fermi-Dirac distribution fit of the density distribution of spin polarised clouds recorded after a 5 ms time-of-flight expansion at a bias field of 300 G. It is important to stress that the final configuration is perfectly symmetric, both in total spin population and density distribution, and each component does not present any appreciable shape nor center-of-mass oscillation within the separated reservoirs. We note here that a measurement of the oscillation frequency of a single spin component within one isolated reservoir yields $\nu_R = 1.78(5)\nu_z$. This is only about 10% lower than the value $2\nu_z$ expected for the case of an infinitely thin barrier. This justifies the approximation of the barrier potential as delta-like for modelling the cloud density, as discussed in detail in the following.

Excitation and measurement of the spin-dipole oscillations
In order to excite the spin-dipole mode at a given Feshbach field, we rapidly turn off the barrier potential from its maximum height of about $10E_F$ down to zero, within less than one μs. At the start, when the Gaussian barrier has its maximum height, the two spin clouds have an initial separation of the order of 5 μm, and the sudden release of the barrier causes the two domains to expand one towards the other at a small, though non-zero, relative velocity. From here on, we monitor the dynamics of the relative distance between the center-of-mass of the two clouds. For each value of evolution time, in two independent and successive experimental runs, we acquire two *in situ* absorption images, each of which is resonant only with one spin state. For each point of interaction, temperature, and evolution time herein investigated, the relative distance between the centres of the two clouds is determined by averaging over at least five independent measurements. The determination of the center of mass of each cloud is obtained either via a Gaussian fit to the imaged density distribution $n_{2D,\sigma}(y,z)$ with $\sigma = \uparrow, \downarrow$, or via the evaluation of the center-of-mass of each sample obtained via direct integration of the bare images: $z_\sigma = \int z\, n_{2D,\sigma}(y,z)\, dy\, dz / N_\sigma$. Once the spin dynamics is recorded, we fit $d(t) = (z_\uparrow - z_\downarrow)(t)$ to an exponential decay. By subtracting the fitted exponential decrease of $d(t)$ due to diffusion from the data, we obtain a measure of the spin dipole mode, whose frequency is extracted from the data by means of a damped sinusoidal function $f(t) = A\cos(2\pi\nu_s\, t)\, e^{-t/\tau}$. Besides exciting the spin dipole mode, our experimental protocol also excites weakly the breathing mode, which is detected by studying the evolution of the axial and radial widths of the two clouds. Similarly to what done for the center-of-mass separation dynamics, we characterise the breathing oscillation by subtracting to $\sigma_z(t)$ an overall exponential drift and fitting the residual modulation $\Delta\sigma_z(t)$ with a damped sinusoidal function, as in Fig. 6. For weak interactions, the breathing mode oscillates at twice the axial trap frequency ν_z, as expected for a collisionless regime. Increasing the interaction strength, we observe a transition to a hydrodynamic regime, characterised by a decrease of the breathing mode frequency ν_B down to $\sqrt{12/5}\nu_z$. Performing an analysis similar to the one reported by Gensemer *et al.*[32], the trends of both the frequency and damping rate of the breathing mode show the transition to occur already for $\kappa_F a \geq 0.2$, as shown in Fig. 6b,c. In the strongly interacting regime ($\kappa_F a \geq 1$), where the ferromagnetic instability is detected, the amplitude of the breathing mode is extremely small, generally around 2% of the size of the cloud.

Based on the measured trend of the breathing mode frequency and damping, it is therefore clear that neither the observed softening of the spin-dipole mode below the ferromagnetic instability nor its sudden frequency increase can be ascribed to the collisionless-to-hydrodynamic transition, the latter occurring already for much weaker interactions, as shown in Fig. 6b,c.

Measurement of spin transport
As already mentioned in the main text, to investigate the plateau in the spin dynamics and in general for measuring the spin drag coefficient, we employ a different protocol that allows us not to initially excite spin-dipole oscillations. For these measurements, we turn off the barrier in a two-stage

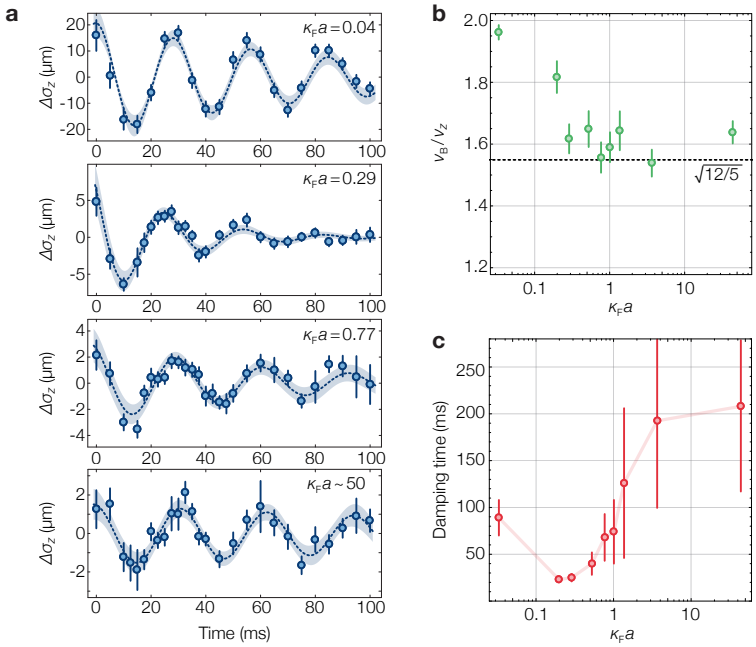

FIG. 6. Transition from collisionless to hydrodynamic regime in the axial breathing mode. (a) Evolution of the axial breathing mode for different interaction strengths at $T/T_F = 0.12(2)$ after a sudden barrier switch-off. (b) Normalised breathing frequency as a function of $\kappa_F a$. The breathing mode frequency decreases from twice the axial trap frequency and, at $\kappa_F a \simeq 0.2$, it approaches $\nu_B/\nu_z \simeq \sqrt{12/5}$. (c) Damping time of the breathing mode versus $\kappa_F a$. The transition from a collisionless to a hydrodinamic regime is additionally detected through the damping time, which reaches a minimum at $k_F a \simeq 0.2$.

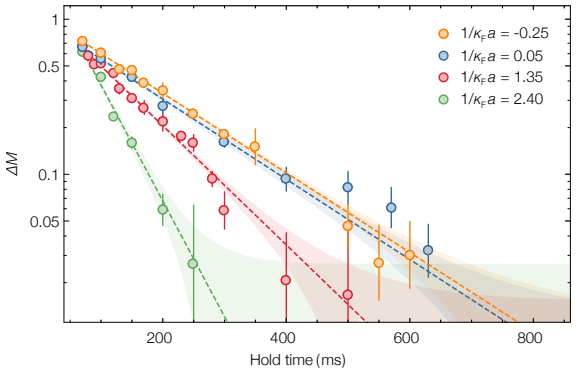

FIG. 7. Spin diffusion dynamics at hold times $t > 50$ ms for $T/T_F = 0.12(2)$. The evolution of the magnetisation $\Delta M(t)$ is plotted for various interaction strengths. Data points averaged over 4-5 indipendent experimental realizations (with error bars representing the s.e.m. of the data) are shown together with fits to the solution of the simple kinetic model from which we extract Γ_S (see Eq. (27)).

sequence. First, we lower the repulsive barrier from $10\,E_F$ down to about $\leq 2\,E_F$ with a linear ramp lasting 30 ms (see Fig. 5c). The ramp speed and final barrier height are chosen to ensure an adiabatic re-adjustment of the density distributions of the two clouds in the barrier region, while preventing a detectable tunnelling of atoms across the barrier and not inducing any shape excitations. In this way, the magnetization in each reservoir does not change, but the relative distance between the edges of the two spin domains near $z = 0$ is drastically reduced, from 5 μm down to about 1 μm, a length-scale comparable with the mean interparticle spacing of our gas at the interface.

In a second stage, we ramp the intensity of the repulsive barrier down to zero. We have investigated different durations of the second ramp, spanning from 0 up to 30 ms. For times between 10 and 30 ms, we detect an appreciable flow of atoms across the barrier region already during the ramp. In this case, once the barrier is off, the spin dynamics is well described by a continuous, single exponential decay (see Fig. 7). For ramps shorter than 10 ms, in the strongly interacting regime, we observe a $\tau_p > 0$ window of vanishing spin diffusion. For ramp times below 5 ms, the duration of the plateaus is maximised and, for each target field explored in this work, it does not show any dependence on the ramp speed. For the measurements presented in Fig. 3 and 4 of the main text, the barrier is turned off in 5 ms.

II. EFFECTIVE FERMI ENERGY AND FERMI WAVEVECTOR

In order to account for the inhomogeneity, the finite temperature, and the initial density of the two spin components in disconnected reservoirs, in the main text we have defined κ_F and ϵ_F as relevant length and energy scales. These are evaluated by approximating the thin barrier at $z = 0$ as a delta-like potential. As already discussed in Section I, this is a reasonable assumption, considering that the barrier thickness of 2 μm is about 70 times smaller than the typical Thomas-

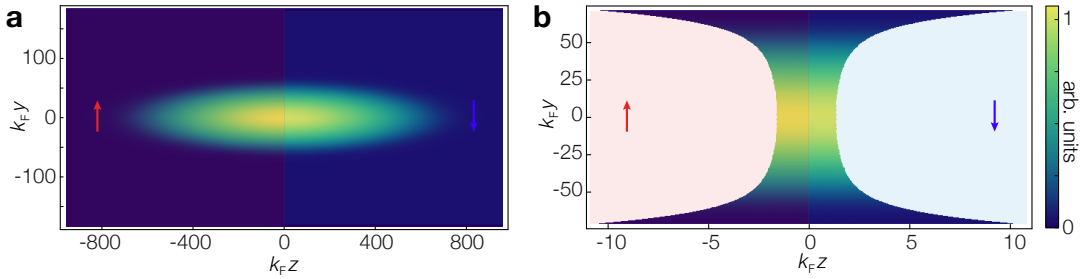

FIG. 8. (a) Model for total density distribution of the initial state: the optical barrier is approximated as infinitely thin, and the total profile of the two spin components is given by the one of a Fermi gas of $N_\uparrow + N_\downarrow$ atoms at the given temperature, occupying the whole trap. (b) The values of the effective Fermi energy ϵ_F and wave vector κ_F are obtained by averaging over a slice around $z = 0$ of total thickness equal to one (local) interparticle spacing.

Fermi radius of the cloud along the z axis. This is also confirmed by the measurement of the oscillation frequency within each reservoir, that is found to be $\sim 10\%$ lower than the value $2\nu_z$ expected for the case of a delta-like potential. Namely, we approximate the density distribution of a Fermi gas of N atoms confined in "half" a harmonic trap as half of the distribution of a Fermi gas of $2N$ atoms occupying the whole dipole trap. This is evaluated with a finite temperature Fermi-Dirac distribution of an ideal Fermi gas $n_F(\mathbf{r}, T/T_F)$, given the measured T/T_F, trap frequencies, and atom numbers, see Fig. 8a. The obtained profile excellently reproduces the two $\uparrow$ and $\downarrow$ clouds, imaged *in situ* independently. From $n_F(\mathbf{r}, T/T_F)$ the local Fermi energy and wavevector are given respectively by $k_F(\mathbf{r}, T/T_F) = (6\pi^2 n_F(\mathbf{r}, T/T_F))^{1/3}$ and $E_F(\mathbf{r}, T/T_F) = \hbar^2 k_F(\mathbf{r}, T/T_F)^2/(2m_{\rm Li})$.

The two parameters κ_F and ϵ_F are derived by averaging the local $k_F(\mathbf{r}, T/T_F)$ and $E_F(\mathbf{r}, T/T_F)$ over one interparticle spacing $(6\pi^2)^{1/3}/k_F(x, y, 0, T/T_F)$ around $z = 0$, see Fig. 8b. Parallel to this, integration of $n_F(\mathbf{r}, T/T_F)$ within this region yields the total number N_{int} of $\uparrow$ and $\downarrow$ fermions at the interface between the two pseudospin domains. The definition of such an energy- and length-scale are inspired by a recent study on the spatial distribution of a fully ferromagnetic two-fermion mixture in a harmonic trap[33], which predicts that the domain wall at the interface between the two magnetic domains has a total thickness of one interparticle spacing.

III. SUM-RULE APPROACH FOR THE PREDICTION OF SPIN-DIPOLE FREQUENCY

As emphasized in the main text, the measured out-of-phase oscillation frequency compares very well with a theoretical estimate based on a sum-rule approach supplemented with quantum Monte Carlo (QMC) data and employing a local density approximation[10].

The sum-rule approach is a very powerful method to give an upper bound of collective modes in confined systems[34]. It is based on the knowledge of different momenta of the linear response of the system to the perturbation exciting the mode of interest. If the perturbation operator is D, the moments of the strength distribution function, or sum rules, are given by $m_k = \sum_n |\langle 0|D|n\rangle|^2 (E_n - E_0)^k$. An upper bound to the mode frequency is provided by the ratios of the sum rules.

The out-of-phase, or spin-dipole mode in particular is excited by the operator $D = \sum_i (z_{i\uparrow} - z_{i\downarrow})$, where z is the longitudinal coordinate. We estimate the frequency of this oscillation using the ratio

$$\hbar^2 \omega_{SD}^2 = \frac{m_1}{m_{-1}} \tag{5}$$

The reason is two-fold: (i) the inverse energy weighted sum rule m_{-1} is sensitive to low frequencies which dominate since the stronger the repulsive interaction the softer the spin-dipole mode; (ii) m_{-1} is related to the susceptibility of the system.

The so-called energy weighted sum rule m_1 is easily calculated in terms of a double commutator:

$$m_1 = \frac{1}{2}\langle 0|[D,[H,D]]|0\rangle = N\frac{\hbar^2}{2m}. \tag{6}$$

The inverse energy-weighted sum rule is proportional to the spin dipole susceptibility. The latter can be determined by minimizing the total energy of the system in the presence of an external static coupling of the form $-\lambda D$.

Since our system is inhomogeneous we write the energy assuming local density approximation to be valid:

$$E = \int d\mathbf{r}[\epsilon(n_\uparrow(\mathbf{r}), n_\downarrow(\mathbf{r})) - \lambda z(n_\uparrow(\mathbf{r}) - n_\downarrow(\mathbf{r}))] \tag{7}$$

where $\epsilon(n_\uparrow, n_\downarrow)$ is the energy density of uniform matter. By expanding $\epsilon(n_\uparrow, n_\downarrow)$ up to quadratic terms in $n_\uparrow - n_\downarrow$, minimisation of E yields the result $n_\uparrow - n_\downarrow = \lambda z \chi(n)$ for the polarisation induced by the external field. Here $\chi^{-1}(n) = \partial^2\epsilon/\partial(n_\uparrow - n_\downarrow)^2$ is the zero temperature inverse magnetic susceptibility of the uniform matter calculated at the local value of the density. The calculation of the induced spin dipole moment then yields $m_{-1} = 1/2 \int d\mathbf{r} z^2 \chi(n)$ and hence the result

$$\omega_{SD}^2 = \frac{N}{m \int d\mathbf{r} z^2 \chi(n)} \tag{8}$$

for the spin dipole frequency. Eq. (8) is exact within local density approximation and it shows that an increase of the magnetic susceptibility will result in a decrease of ω_{SD}. If

a ferromagnetic transition occurs, the spin-dipole mode frequency shows a minimum associated with a diverging spin susceptibility, occurring within the central high density region of the trap. Once a ferromagnetic domain is formed, Eq. (8) is no longer valid and the dynamical behaviour of the system strongly depends on the geometry of the domain wall itself.

For an ideal Fermi gas trapped in a harmonic potential one gets the simple result $\omega_{SD} = \omega_z$ where ω_z is the trap frequency along the z-axis. For a balanced interacting Fermi gas on the repulsive branch we use both for the energy density and the bulk magnetic susceptibility the QMC results by Pilati *et al.*[18]. Both quantities can be written easily as an expansion in $k_F a$ above the mean-field results:

$$\frac{\epsilon}{\epsilon_0} = 1 + k_F a + C_\epsilon (k_F a)^2 \tag{9}$$

$$\frac{\chi_0}{\chi} = 1 - \frac{2}{\pi} k_F a - C_\chi (k_F a)^2, \tag{10}$$

where ϵ_0 and χ_0 are the chemical potential and the susceptibility of a spin-$1/2$ free Fermi gas, respectively. The constants $C_\epsilon = 0.28$ and $C_\chi = 0.62$ are fitting parameters to the Monte-Carlo results. The previous expressions are suitable to determine an upper bound to the spin-dipole mode frequency for an unpolarised gas at equilibrium in the trap[10].

Providing a rigorous theoretical description of the experimental results shown in Fig. 2 of the main text is challenging since the gas has a time and space dependent local polarisation. However, some comments are due here: (i) the position at which the frequency has an abrupt change (reaches its lowest value) does not depend on the configuration; (ii) our initial configuration enhances the effect with respect to the paramagnetic ground state considered by Recati *et al.*[10]; (iii) the measured frequency should generally be larger than the result of Recati *et al.*[10] since only part of the gas is interacting during the oscillation frequency measurement. We can estimate an upper bound for the frequency by considering a configuration formed by two outer fully polarised regions (free Fermi gases) and an inner unpolarised layer, described by the equation of state Eq. (10). The extension of the inner layer can be assumed to be the region where the two species have a sizeable overlap during the oscillation, which we estimate to be at least 25% of the total length of the cloud. The results are reported in Fig. 2 of the main text as solid (full overlap) and dashed (25% overlap) lines, and are found to mark a confidence region within which all experimental data fall in.

IV. TEMPERATURE SHIFT OF THE CRITICAL INTERACTION STRENGTH

Within Landau theory of Fermi liquid the inverse susceptibility at $T = 0$ can then be written as[35]

$$\chi^{-1}(T=0) = \frac{2}{g(e_F)}(1 + F_0^a) \tag{11}$$

where F_0^a is the $l = 0$ antisymmetric (magnetic) Landau parameter, $g(e_F) = m^* k_F/\pi^2$ is the density of states with $m^* = m(1 + F_1^s/3) > m$ and F_1^s is the $l = 1$ symmetric (density) Landau parameter. To the first order in the interaction one has $m^* = m$ and $F_0^a = -2k_F a/\pi$.

At finite temperature but $T \ll T_F$ we can consider the corrections to previous expression only due to free quasiparticles which is proportional to n, and therefore to T^2. The interaction term depending on n^2 will contribute to higher order $O(T^4)$:

$$\chi^{-1}(T) = \frac{2}{g(e_F)}(1 + F_0^a + \pi^2/12(T/T_F)^2) \tag{12}$$

The paramagnetic state becomes unstable when $\chi^{-1} = 0$, which at zero temperature can occur if there exists a critical value $(k_F a)_c$ such that $F_0^a = -1$. At low T we can expand the Landau parameters around their values at the critical point $(k_F a)_c$ at zero temperature

$$F_0^a = F_{0,c}^a + \left(\frac{\partial F_0^a}{\partial (k_F a)}\right)_c (k_F a - (k_F a)_c) \tag{13}$$

$$F_1^s = F_{1,c}^s + \left(\frac{\partial F_1^s}{\partial (k_F a)}\right)_c (k_F a - (k_F a)_c). \tag{14}$$

Therefore we find that the critical temperature for the paramagnetic state to be unstable can be simply written as

$$\left(\frac{T}{T_F}\right)_c = \frac{2\sqrt{3}}{\pi}\sqrt{-\left(\frac{\partial F_0^a}{\partial (k_F a)}\right)_c}\sqrt{k_F a - (k_F a)_c} \tag{15}$$

For instance using the expression for F_0^a at the second order in $k_F a$ one gets the first correction to the usual expression. In particular $(k_F a)_c \simeq 1.05$ and the critical temperature reads

$$\left(\frac{T}{T_F}\right)_c \simeq \frac{2^{3/2}\sqrt{3}}{\pi^{3/2}}\sqrt{1 + (k_F a)_c \frac{8}{3\pi}(1 - \ln 2)}\sqrt{k_F a - (k_F a)_c} \tag{16}$$

In principle, application of the aforementioned power law as a fit to the experimental data in Fig. 3d (tentative phase diagram) is not justified: in fact, $\tau_p > 0$ is interpreted as the onset of the fully ferromagnetic state, whereas Eq. (15) marks the boundary between para- and partially ferro-magnetic phases. On the other hand, however, all QMC results show that the partially ferromagnetic phase for a homogeneous system occupies a very narrow region of the phase diagram, and we expect that in our trapped system its presence is essentially washed out by the inhomogeneity of the clouds density distribution and finite experimental resolution.

V. PAIRING INSTABILITY AND MOLECULE FORMATION

One major issue that has impeded the observation of the ferromagnetic instability in previous experiments with ultracold Fermi gases[7,8] is represented by the pairing instability[6]. As discussed in the main text, ferromagnetic behaviour develops along the upper branch of the many-body system: however, this state features an additional instability, represented by the tendency of the paramagnetic phase to turn via inelastic processes into a gas of pairs, which represents the true ground

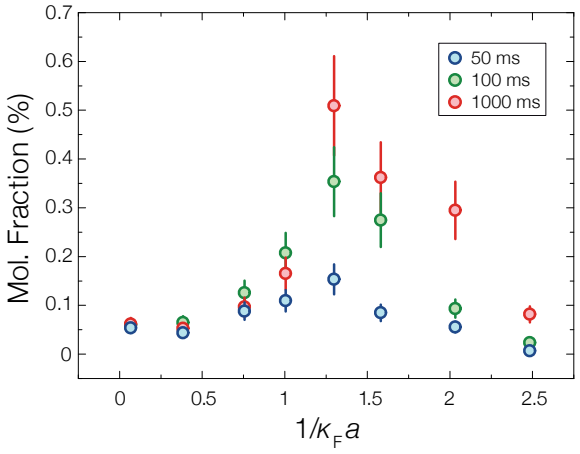

FIG. 9. Measured molecule fraction obtained through the double-pulse imaging technique. The peak of molecule formation appears below the measured critical interactions, at $1/(\kappa_F a) \simeq 1.3$.

state of the balanced system at low temperatures. At least for homonuclear mixtures and broad resonances[6,8,13], the pairing instability always overcomes the Stoner's one. Thanks to our preparation scheme, that artificially initialises the system into a fully ferromagnetic configuration, we are able to contain the system tendency towards pairing, allowing for the investigation of the metastable upper branch. Furthermore, as discussed in Sec. VI, attractive polarons, rather than pairs, seem to be the preferential decay products in our system, at least in the strongly interacting regime. Nonetheless, molecule formation has represented a major issue in previous experiments, and ruling out pairing effects for explaining the dynamics observed in our studies is fundamental for further supporting our interpretation. In previous experiments[8], the population of molecules and atoms has been identified via a rapid magnetic field ramp technique. After some evolution time at a target field close to the Feshbach resonance center, where molecules could be formed via recombination processes, two successive absorption images were acquired. A first, taken at high field, allowed to monitor the total population of atoms and molecules, since the molecule binding energy close to the Feshbach resonance is two to three orders of magnitude smaller than the natural linewidth of the imaging transition. This allows to take a picture of the molecules with the same imaging light employed for the atom, being the latter in the $\uparrow$ or $\downarrow$ state. A second imaging pulse was taken after a rapid sweep of the magnetic field to zero. The ramp converts weakly bound pairs into deeply bound molecules, which become transparent to the atom imaging light. Hence, the second imaging selectively monitors the atom population, i.e. the population of the upper branch. Our setup does not allow to perform fast ($\sim 10^2$ G/μs) ramps to low fields, hence we employed a different protocol to monitor the presence of molecules in the system. This is based on acquiring, within a single experimental run, two subsequent absorption images, by means of 4 μs long pulses resonant with the $\uparrow$ and $\downarrow$ states, respectively, and separated by 300 μs. If no molecules are present, the effect of the first imaging pulse resonant with the $\uparrow$ state on $\downarrow$ atoms is negligible, the $\uparrow$ imaging light being off-resonant to the $\downarrow$ component. Furthermore, the short delay between the two pulses greatly limits the effect of heating of the $\downarrow$ cloud associated to collisions with escaping $\uparrow$ imaged atoms. The effect of the first imaging pulse is in turn completely different if molecules, rather than atoms, are considered. Since the $\uparrow - \downarrow$ dimers are only weakly bound, the first imaging photon, resonant with the $\uparrow$ optical transition, dissociates the bound state into two atomic products[36], each of which symmetrically acquires a significant momentum. The latter is associated to the density of states of the two outgoing atoms, to the binding energy of the dimer (negligible in this case), and to the photon momentum $\hbar k_L$. The increase of the cloud size detected by the second imaging pulse is thus proportional to the amount of molecules in the system. We therefore monitor the increase of the radial width after the first pulse for different interaction strengths and different evolution times during the spin diffusion.

A simple model allows to link the molecular fraction to the increase of the cloud width after the first pulse, following the experimental protocol described above. In general, the size of a trapped cloud can be written as:

$$\langle x_0^2 \rangle = \frac{2\langle U \rangle}{m\omega^2} \tag{17}$$

Where $\langle U \rangle$ is the potential energy of one atom weighted over the density distribution of the cloud, the latter being eventually modified by interaction effects. In the case of a pure gas of dimers, application of an imaging pulse resonant with the $\uparrow$ component causes the dimers to dissociate with a certain transfer of energy E_1 to the $\downarrow$ component. Since the photon energy is always larger than the binding one, we assume E_1 to be independent from the molecular binding, and hence independent from $\kappa_F a$.
According to the same argument of Eq. (17), the width measured through the second pulse, following the first, can be written as:

$$\langle x_1^2 \rangle = \frac{2\langle U + E_1 \rangle}{m\omega^2} \tag{18}$$

If the gas is a mixture of free atoms and molecules, the mean size is set by:

$$\langle x^2 \rangle = \frac{N_a \langle x_0^2 \rangle + N_m \langle x_1^2 \rangle}{N_a + N_m} \tag{19}$$

Defining the molecular fraction $f_m = N_m/N$, we get:

$$\langle x^2 \rangle = \frac{2}{m\omega^2}\langle U \rangle + \frac{2}{m\omega^2}\langle E_1 \rangle f_m = \langle x_0^2 \rangle + \frac{2}{m\omega^2}\langle E_1 \rangle f_m \tag{20}$$

When starting from a pure molecular sample, $f_m = 1$, we would have:

$$\frac{2}{m\omega^2}\langle E_1 \rangle = \langle x_{1m}^2 \rangle - \langle x_{0m}^2 \rangle \tag{21}$$

We can therefore express the molecular fraction as:

$$f_m = \frac{\langle x_1^2 \rangle - \langle x_0^2 \rangle}{\langle x_{1m}^2 \rangle - \langle x_{0m}^2 \rangle} \tag{22}$$

The denominator of Eq. (22) can be experimentally determined by applying the double-pulse imaging technique on a BEC-BCS crossover superfluid at a temperature $T/T_F < 0.1$, which ensures a molecular fraction $f_m \simeq 1$ on the BEC side of the resonance. The change of the density distribution when moving from the unitary limit to the BEC one is accounted by renormalizing the measured radial width by the average density of the gas, evaluated with the conventional single-pulse absorption imaging.
The numerator of Eq. (22) is evaluated by measuring the radial size of the cloud $\langle x_1^2 \rangle$ at different evolution times of the dynamics. Conversely, $\langle x_0^2 \rangle$ is the size measured through the first imaging pulse at the corresponding times. Results of this analysis are reported in Fig. 9, for various interaction strengths and different diffusion times, for a repulsive Fermi gas mixture initially prepared at T/T$_F$=0.12(2).

The general trend for these measurements is interpreted as follows: starting from the weakly repulsive regime, the upper branch is very long-lived, and despite rapid mixing of the two spin clouds only a small number of molecules is formed. Increasing interactions, the decay rate of the upper branch monotonically increases[13,22,28,37]: hence, despite a parallel increase of the spin drag coefficient[11,26], which tends to slow down the interpenetration and to reduce the spatial overlap of the $\uparrow$ and $\downarrow$ clouds, the molecule formation becomes more sizable, reaching a maximum near $1/(\kappa_F a) \simeq 1.3$, in good agreement with Ref. 33. However, as one accesses the strongly interacting regime where the magnetic susceptibility is increasing, the molecule formation is again strongly reduced, highlighting the resistance of the system to mix the two spin components. The trend at large $\kappa_F a$ values, observed also after long evolution times even when the spatial overlap of the two clouds has considerably increased, suggests that also at small values of local population imbalance the system may be a Fermi liquid state of attractive polarons, rather than a Bose gas of dimers. The Fermi liquid state might be favored by our way to initialize the system dynamics, and also by the temperature increase associated to the exothermic decay process from the upper to the lower branch.

Importantly, for timescales below 100 ms, over which both the plateau measurements and the spin-dipole oscillations were acquired, the observed heating is relatively small and the derived molecule fraction remains below 10% for interaction strengths exceeding the critical value for the stop of diffusion to occur. We therefore conclude that neither the behaviour of the spin-dipole frequency nor the appearance of plateaus in the spin diffusion can be strongly influenced by dimer formation. For what concerns the measurement of the spin-dipole frequency, the possible development of a sizeable cloud of molecules is expected to strongly reduce the amplitude of the out-of-phase oscillation. While some additional damping associated to pairing effects cannot be excluded in our frequency measurements, we do not envision how the observed dynamics could arise from a lower-branch energy functional, with attractive interactions forming bound pairs[38,39]. This is equally true if an attractive Fermi liquid, rather than a Bose gas of pairs, would be considered: for this latter system, both experimental studies[39,40] and theoretical calculations[41] indicate that the spin susceptibility monotonically decreases when moving from the BCS to the BEC side of the crossover, vanishing at $k_F a \sim 1$. This in turn would correspond to a spin-dipole frequency monotonically increasing when passing from BCS to BEC side along the lower branch, a qualitatively different trend with respect to the one revealed in our experiment.

VI. PHENOMENOLOGICAL MODEL FOR THE MELTING OF THE DOMAIN WALL

In this section, we describe the phenomenological model developed to explain the finite duration of the plateau in the spin diffusion, as a function of the interaction and temperature. Such a model is based on the precise knowledge[28] of the spectral properties and lifetime of $\downarrow$ impurities embedded in a Fermi sea of $\uparrow$ particles. As discussed in the main text, the spectral function of such system is characterised by an upper and a lower branch. Depending on the interaction strength, associated to the lower branch there exist in the extremely imbalanced case two kinds of Landau's quasiparticles, coined attractive polarons and dressed molecules[13]. For interaction parameters $1/(\kappa_F a) > 0.9$ ($1/(\kappa_F a) < 0.9$) dressed molecules (attractive polarons) represent the absolute ground state of the many-body system. The upper branch, in turn, features a third kind of quasi-particle, the repulsive polaron, whose existence has been recently experimentally demonstrated investigating both a three-dimensional mass-imbalanced Fermi mixture of ^{40}K and ^{6}Li atoms[22], and also a two-dimensional Fermi mixture of ^{40}K atoms[42]. While the lower branch is associated to a net attractive interaction between the impurity and the particles of the medium, the upper one requires repulsion between the two species in order to develop. For increasing repulsive interaction ($1/(\kappa_F a) \to 0^+$), the energy of the repulsive polaron progressively increases. However, parallel to this, the repulsive polaron acquires a progressively shorter lifetime, set by the tendency of the system to decay onto the lower-lying states of the attractive branch. It can be shown[13,22] that the main decay mechanism that destabilize the repulsive branch is associated with relaxation into attractive polarons, rather than into dressed molecules. The decay rate Γ associated with such an inelastic process, together with the energy E_+ and E_- of the repulsive and attractive branch, has been determined via recent non-perturbative theory approaches[13,28].

Although our system is a 50-50 balanced mixture of $\uparrow$ and $\downarrow$ fermions, the results obtained in the impurity limit are extremely relevant for understanding the existence of a plateau of zero diffusivity in the spin dynamics. Since our studies start by preparing a fully ferromagnetic phase-separated state, rather than a mixed paramagnetic phase, the initial mixing processes at the interface between the two spin domains can be envisioned as events in which fermions of one kind enter in the Fermi sea of the other component, and vice-versa. Those are well describable in terms of the properties of dressed quasiparticles derived in the impurity limit.

Our proposed explanation of the conductance plateau shown in Fig. 3 of the paper proceeds along the following

line of thought. In the case of purely repulsive interaction, the ferromagnetic state, if energetically allowed, would be indefinitely stable, and in a system with separately fixed spin populations would correspond to a phase-separated state. In fact, the miscibility of the two components would be prevented by the existence of a domain wall: namely, a $\downarrow$ fermion at the interface would need to pay a finite amount of energy $\sigma > 0$ in order to access the other spin domain forming a repulsive polaron. In our metastable system, however, if a repulsive polaron is created, it can subsequently decay onto the lower branch with a rate Γ, releasing an energy equal to the mismatch between the two branches, $E_+ - E_-$. Hence, this two-step process will cause a net increase of energy $\Delta E = E_+ - E_- - \sigma$ at a rate Γ. We assume that at the beginning of the dynamics, the energy associated to the domain wall is given by σN_{int}, N_{int} being the total number of fermions within a slice around $z = 0$ of total thickness equal to one interparticle spacing, see Section II. The duration of the plateau τ_p is then set by the condition:

$$\sigma N_{int} = (E_+ - E_- - \sigma)\tau_p \Gamma \tag{23}$$

Phenomenologically, we assume that $\sigma = E_+ - E_{+c}$, where E_+ is the energy of a repulsive polaron, while E_{+c} is the energy of one free fermion at the interface. In homogeneous systems and in the impurity limit[13], $E_{+c} = E_F$. In our inhomogeneous sample, and in the vicinity of the interface between the two spin clouds, we introduce E_{+c} as a phenomenological parameter.

Consequently, from Eq. (23) we obtain the following expression for τ_p:

$$\tau_p = \frac{N_{int}(E_+ - E_{+c})}{\Gamma(E_{+c} - E_-)} \frac{1}{2\pi\nu_F} \tag{24}$$

where $h\nu_F = \epsilon_F$.

To compare the prediction of Eq. (24) to our data we employ the values of E_+, E_- and Γ given as a function of the interaction by Schmidt *et al.*[28], and the values of κ_F, ϵ_F and N_{int} obtained after radial averaging over finite temperature density profiles as described in Section II. The only free parameter of the model, E_{+c}, is fixed by optimizing the agreement between experimental data and the prediction of Eq. (24).

It is worth stressing how such a simple theory model, which accounts for finite temperature effects only via a renormalization of κ_F, ϵ_F and N_{int} evaluated at the interface between the two spin domains, is able to provide a quantitative description of the experimentally observed trend.

The model prediction stops at the unitary point and does not extend on the $a < 0$ side of the Feshbach resonance, because the theory becomes not reliable in this region, the decay rate of the upper branch becoming on the order of the Fermi energy, hence making the repulsive polaron an ill-defined quasiparticle[28]. While the spin dynamics on the BCS regime definitively deserves further deeper theoretical and experimental investigation, both τ_p and ν_s trends at low temperatures are consistent with the picture that the system temporarily access the upper branch even on the $\kappa_F a < 0$ side of the Feshbach resonance. This extremely exotic many-body state, which is a three-dimensional analogue of the super-Tonks regime in one dimension[43], is thus far poorly explored even in theory and will be the subject of future studies.

VII. THEORY MODEL FOR THE DIFFUSION OF ONE ATTRACTIVE POLARON

The equation for the dynamics of the relative center of mass $d(t) = z_\uparrow - z_\downarrow$ can be easily obtained starting from the Boltzmann equation and using the method of the averages[44]. One obtains the following coupled equations

$$\begin{aligned} \partial_t(z_\uparrow - z_\downarrow) - (v_\uparrow - v_\downarrow) &= 0 \\ \partial_t(v_\uparrow - v_\downarrow) + \omega_z^2(z_\uparrow - z_\downarrow) &= (\partial_t(v_\uparrow - v_\downarrow))_{coll}, \end{aligned} \tag{25}$$

where ω_z is the trapping frequency in the direction of the motion, $v_\uparrow$ ($v_\downarrow$) is the average velocity of the $\uparrow$ ($\downarrow$) spin component and $(\partial_t(v_\uparrow - v_\downarrow))_{coll}$ is the collisional term. The effect of the medium is included in this approach only in the collisional term. Assuming that the distribution function changes in time only through the change of velocity, the collisional term is simply proportional to the relative velocity and can be written as

$$(\partial_t(v_\uparrow - v_\downarrow))_{coll} = -\Gamma_S(v_\uparrow - v_\downarrow), \tag{26}$$

where Γ_S is the so-called spin drag coefficient. Therefore, substituting Eq. (26) in Eq. (25) the equation of motion for d is simply given by the one of a damped harmonic oscillator:

$$\ddot{d} + \Gamma_S \dot{d} + \omega_z^2 d = 0 \tag{27}$$

The theoretical task is to determine the spin drag. For $\downarrow$ impurities moving through a fully polarized noninteracting $\uparrow$ Fermi sea, the drag rate can be computed as

$$\begin{aligned} \hbar\Gamma_S = \frac{2\pi}{k_B T n_\downarrow} \int \frac{d^3p_1}{(2\pi\hbar)^3} \frac{d^3p_2}{(2\pi\hbar)^3} \frac{d^3p_3}{(2\pi\hbar)^3} \, \delta(\varepsilon_1 + \varepsilon_2 - \varepsilon_3 - \varepsilon_4) \\ \times \frac{(4\pi\hbar^2)^2}{m^2} \frac{d\sigma}{d\Omega} \, p_{1j}(v_{1j} - v_{3j}) \, n_{1\downarrow} n_{2\uparrow}(1 - n_{3\downarrow})(1 - n_{4\uparrow}). \end{aligned} \tag{28}$$

This collision integral describes the scattering of an impurity atom with momentum $\vec{p}_1$ and a medium atom with momentum $\vec{p}_2$ into outgoing states $\vec{p}_3$ and $\vec{p}_4 = \vec{p}_1 + \vec{p}_2 - \vec{p}_3$, conserving the total momentum and the total kinetic energy $\varepsilon_1 + \varepsilon_2$ of both particles. Each particle has kinetic energy $\varepsilon_{\vec{p}} = p^2/2m$ and mass m. The drag rate is proportional to the change in impurity velocity, $v_{1j} - v_{3j}$, where j denotes the spatial component in the direction of the initial impurity velocity. The scattering process occurs with probability $n_{1\downarrow} n_{2\uparrow}$ that the initial states are occupied, and probability $(1 - n_{3\downarrow})(1 - n_{4\uparrow})$ that the final states are unoccupied, where $n_{\vec{p}\sigma} = [\exp(\beta(\varepsilon_{\vec{p}\sigma} - \mu_\sigma)) + 1]^{-1}$ is the Fermi-Dirac distribution at chemical potential μ_σ. The drag rate Eq. (28) is derived from spin diffusion theory for a polarized Fermi gas[45–47] in the limit of vanishing minority density $n_\downarrow$ (the integral over the impurity distribution $n_{1\downarrow}$ cancels the factor $n_\downarrow$ in the denominator of Eq. (28) to yield a

finite drag rate). Equivalently, Eq. (28) is obtained from the impurity drag rate[26,48] in the limit of vanishing impurity velocity.

In order to compute the cross section $d\sigma/d\Omega$ for a dilute Fermi gas we use the T matrix in the ladder approximation[49]. In an ultracold Fermi gas the bare interaction is an s-wave contact interaction between unequal spins, thus also the T matrix only has an s-wave component $\ell = 0$. One can then express the differential cross section

$$\frac{d\sigma}{d\Omega} = |f_{\ell=0}(\vec{q},\omega)|^2 \tag{29}$$

in terms of the s-wave scattering amplitude $f_{\ell=0}(\vec{q},\omega)$ of two incoming particles with total momentum $\vec{q} = \vec{p}_1 + \vec{p}_2$ and total kinetic energy $\hbar\omega = \varepsilon_{\vec{p}_1\uparrow} + \varepsilon_{\vec{p}_2\downarrow}$. The scattering amplitude, in turn, is given in terms of the T matrix $\mathcal{T}_\ell$ as[49]

$$f_{\ell=0}(\vec{q},\omega) = -\frac{mQ}{4\pi\hbar^2}\,\mathcal{T}_{\ell=0}(\vec{q},\omega). \tag{30}$$

For two particles scattering in vacuum ($Q = 1$), the two-body T matrix reads

$$\mathcal{T}^{(0)}_{\ell=0}(\vec{q},\omega) = \frac{4\pi\hbar^2 a/m}{1+iak} \tag{31}$$

where a denotes the s-wave scattering length, and $\hbar\vec{k} = (\vec{p}_1 - \vec{p}_2)/2$ is the relative momentum of incoming particles. This results in a vacuum scattering amplitude $f^{(0)}_{\ell=0} = -a/(1+iak)$ and vacuum scattering cross section $d\sigma^{(0)}/d\Omega = |f^{(0)}_{\ell=0}|^2 = a^2/(1+a^2k^2)$. At weak coupling $|k_{F\uparrow}a| \ll 1$, the drag rate is proportional to the scattering cross section, $1/\tau_p \propto a^2$. Note that with the vacuum cross section, the drag rate depends only on the modulus $|a|$ of the scattering length and is symmetric in a around unitarity ($a^{-1} = 0$) in the BCS-BEC crossover. The experimental data for the drag rate, however, exhibit an asymmetry in a. A similar asymmetry in transport coefficients has been observed in the shear viscosity[29] and transverse spin diffusion[30].

In order to explain the asymmetry in the drag rate it is necessary to include medium scattering, where the Fermi sea is Pauli blocked for intermediate states, and which entails a tendency toward molecule formation on the BEC side[50–52]. Medium scattering is described by the many-body T matrix $\mathcal{T}_\ell$,

$$\mathcal{T}^{-1}_{\ell=0}(\vec{q},\omega) = \mathcal{T}^{(0)-1}_{\ell=0}(\vec{q},\omega) + \int \frac{d^3p}{(2\pi\hbar)^3}\,\frac{n_{\vec{p}\downarrow} + n_{\vec{q}-\vec{p}\uparrow}}{\omega - \varepsilon_{\vec{p}\downarrow} - \varepsilon_{\vec{q}-\vec{p}\uparrow} + i0}\,. \tag{32}$$

The medium T matrix includes the effect of quantum degeneracy, which leads to a large increase in the partial-wave scattering amplitudes (30) and would by itself violate the unitarity bound

$$|kf_\ell| \le 1, \tag{33}$$

which is the prerequisite for expressing the scattering amplitude $kf_\ell = e^{i\delta_\ell}\sin\delta_\ell$ in terms of real phase shifts $\delta_\ell(\vec{q},\omega)$. The definition of the scattering amplitudes (30) in the presence of the medium therefore includes a phenomenological Q factor which accounts for the fact that only unoccupied states are available for outgoing waves[49] (Pauli blocking),

$$Q = \int_{-1}^{1} \frac{d\cos\theta}{2}\left(1 - n_{\vec{q}/2+\hbar\vec{k}\downarrow} - n_{\vec{q}/2-\hbar\vec{k}\uparrow}\right). \tag{34}$$

The integral averages over the angle θ between total momentum $\vec{q}$ and relative momentum $\hbar\vec{k}$, while the modulus of $\vec{k}$ is fixed by the condition $\hbar\omega = \varepsilon_{\vec{q}/2+\hbar\vec{k}\downarrow} + \varepsilon_{\vec{q}/2-\hbar\vec{k}\uparrow} = \hbar^2k^2/m + q^2/4m$. In vacuum $Q = 1$, and also at high temperatures $T \gg T_{F\uparrow}$ one has $Q \approx 1$. However, in a degenerate Fermi gas $Q < 1$ lowers the scattering amplitude sufficiently to always satisfy the unitarity bound (33) also in the case of medium scattering.

The drag rate Eq. (28) is known analytically in the whole BCS-BEC crossover in the high-temperature limit $T \gg T_{F\uparrow}$ where the majority Fermi gas is non-degenerate[47],

$$\left(\frac{\hbar\Gamma_S}{E_{F\uparrow}}\right)_{\text{hightemp}} = \frac{16\sqrt{2}}{9\pi^{3/2}}\left(\frac{T_{F\uparrow}}{T}\right)^{1/2}\left[1 - x - x^2e^x\mathrm{Ei}(-x)\right]_{x=\hbar^2/(ma^2k_BT)} \tag{35}$$

where Ei denotes the exponential integral. In this regime, the medium factor $Q = 1$. Conversely, medium scattering becomes important in a degenerate Fermi gas ($T \lesssim T_{F\uparrow}$). In general, the collision term in Eq. (28) can be reduced to a three-dimensional integral which is readily evaluated numerically. The resulting drag rate exhibits a maximum slightly on the BEC side of the resonance, in agreement with our experimental results. As the temperature is increased, the maximum shifts toward unitarity in agreement with the high-temperature expression (35) which is symmetric in a.

[1] Vollhardt, D., Blumer, N. & Kollar, M. Metallic ferromagnetism – An electronic correlation phenomenon. vol. 580 of *Lecture Notes in Physics* (Springer, Heidelberg, Germany, 2001).

[2] Brando, M., Belitz, D., Grosche, F. M. & Kirkpatrick, T. R. Metallic quantum ferromagnets. Preprint at http://arxiv.org/abs/1502.02898. Accepted for publication in *Rev. Mod. Phys.* (2016).

[3] Silverstein, S. D. Criteria for Ferromagnetism in dense neutron Fermi liquids-neutron stars. *Phys. Rev. Lett.* **23**, 139 (1969).

[4] Tatsumi, T. Ferromagnetism of quark liquid. *Phys. Lett. B* **489**, 280 (2000).

[5] Stoner, E. Atomic moments in ferromagnetic metals and alloys

with non-ferromagnetic elements. *Philos. Mag.* **15**, 1018 (1933).

[6] Pekker, D., Babadi, M., Sensarma, R., Zinner, N., Pollet, L., Zwierlein, M. & Demler, E. Competition between pairing and ferromagnetic instabilities in ultracold fermi gases near Feshbach resonances. *Phys. Rev. Lett.* **106**, 050402 (2011).

[7] Jo, G., Lee, Y., Lee, Y., Choi, J., Christensen, C. A., Kim, T. H., Thywissen, J. H., Pritchard, D. E. & Ketterle, W. Itinerant ferromagnetism in a Fermi gas of ultracold atoms. *Science* **325**, 1521 (2009).

[8] Sanner, C., Su, E. J., Huang, W., Keshet, A., Gillen, J. & Ketterle, W. Correlations and pair formation in a repulsively interacting Fermi gas. *Phys. Rev. Lett.* **108**, 240404 (2012).

[9] Lee, Y., Heo, M., Choi, J., Wang, T. T., Christensen, C. A., Rvachov, T. M. & Ketterle, W. Compressibility of an ultracold Fermi gas with repulsive interactions. *Phys. Rev. A* **85**, 063615 (2012).

[10] Recati, A. & Stringari, S. Spin fluctuations, susceptibility and the dipole oscillation of a nearly ferromagnetic Fermi gas. *Phys. Rev. Lett.* **106**, 080402 (2010).

[11] Sommer, A., Ku, M., Roati, G. & Zwierlein, M. Universal spin transport in a strongly interacting Fermi gas. *Nature* **7342**, 201 (2011).

[12] Enss, T. & Haussmann, R. Quantum mechanical limitations to spin diffusion in the unitary Fermi gas. *Phys. Rev. Lett.* **109**, 195303 (2012).

[13] Massignan, P., Zaccanti, M. & Bruun, G. M. Polarons, dressed molecules, and itinerant ferromagnetism in ultracold Fermi gases. *Rep. Prog. Phys.* **77**, 034401 (2014).

[14] Vollhardt, D., Wölfle, P. The superfluid phases of Helium-3. (Taylor and Francis, 1990).

[15] Duine, R. A. & MacDonald, A. H. Itinerant ferromagnetism in an ultracold atom Fermi gas. *Phys. Rev. Lett.* **95**, 230403 (2005).

[16] LeBlanc, L. J., Thywissen, J. H., Burkov, A. A. & Paramekanti, A. Repulsive Fermi gas in a harmonic trap: Ferromagnetism and spin textures. *Phys. Rev. A* **80**, 013607 (2009).

[17] Conduit, G. J., Green, A. G. & Simons, B. D. Inhomogeneous phase formation on the border of itinerant ferromagnetism. *Phys. Rev. Lett.* **103**, 207201 (2009).

[18] Pilati, S., Bertaina, G., Giorgini, S. & Troyer, M. Itinerant ferromagnetism of a repulsive atomic Fermi gas: A quantum Monte Carlo study. *Phys. Rev. Lett.* **105**, 030405 (2010).

[19] Chang, S., Randeria, M. & Trivedi, N. Ferromagnetism in the upper branch of the Feshbach resonance and the hard-sphere Fermi gas. *Proc. Nat. Acad. Sci.* **108**, 51 (2011).

[20] Chin, C., Grimm, R., Julienne, P. S. & Tiesinga, E. Feshbach resonances in ultracold gases. *Rev. Mod. Phys.* **82**, 1225–1286 (2010).

[21] Shenoy, V. B., & Ho, T. Nature and properties of a repulsive fermi gas in the upper branch of the energy spectrum. *Phys. Rev. Lett.* **107**, 210401 (2011).

[22] Kohstall, C., Zaccanti, M., Jag, M., Trenkwalder, A., Massignan, P., Bruun, G. M., Schreck, F. & Grimm, R. Metastability and coherence of repulsive polarons in a strongly interacting Fermi mixture. *Nature* **485**, 615 (2012).

[23] Burchianti, A., Valtolina, G., Seman, J. A., Pace, E., De Pas, M., Inguscio, M., Zaccanti, M. & Roati, G. Efficient all-optical production of large ^{6}Li quantum gases using D_1 gray-molasses cooling. *Phys. Rev. A* **90**, 043408 (2014).

[24] Valtolina, G., Burchianti, A., Amico, A., Neri, E., Xhani, K., Seman, J. A., Trombettoni, A., Smerzi, A., Zaccanti, M., Inguscio, M. & Roati, G. Josephson effect in fermionic superfluids across the BEC-BCS crossover. *Science* **350**, 1505 (2015).

[25] Zürn, G., Lompe, T., Wenz, A. N., Jochim, S., Julienne, P. S. & Hutson, J. M. Precise characterization of ^{6}Li Feshbach resonances using trap-sideband-resolved RF spectroscopy of weakly bound molecules. *Phys. Rev. Lett.* **110**, 135301 (2013).

[26] Duine, R. A., Polini, M., Stoof, H. T. C. & Vignale, G. Spin Drag in an ultracold Fermi gas on the verge of ferromagnetic instability. *Phys. Rev. Lett.* **104**, 220403 (2010).

[27] Taylor E., Zhang S., Schneider W., & Randeria M. Colliding clouds of strongly interacting spin-polarized fermions. *Phys. Rev. A* **84**, 063622 (2013).

[28] Schmidt, R. & Enss, T. Excitation spectra and RF response near the polaron-to-molecule transition from the functional renormalization group. *Phys. Rev. A* **83**, 063620 (2011).

[29] Elliott, E., Joseph, J. A., & Thomas, J. E. Anomalous minimum in the shear viscosity of a Fermi gas. *Phys. Rev. Lett.* **113**, 020406 (2014).

[30] Trotzky, S., Beattie, S., Luciuk, C., Smale, S., Bardon, A. B., Enss, T., Taylor, E., Zhang, S., & Thywissen, J. H. Observation of the Leggett-Rice effect in a unitary Fermi gas. *Phys. Rev. Lett.* **114**, 015301 (2015).

[31] Pilati, S., Zintchenko, I. & Troyer, M. Ferromagnetism of a repulsive atomic Fermi gas in an optical lattice: A quantum Monte Carlo study. *Phys. Rev. Lett.* **112**, 015301 (2014).

[32] S.D. Gensemer and D.S. Jin, *Transition from Collisionless to Hydrodynamic Behavior in an Ultracold Fermi Gas*, Phys. Rev. Lett, **87**, 173201, (2001).

[33] Zintchenko, I., Wang, L. & Troyer, M. Ferromagnetism of the Repulsive Atomic Fermi Gas: three-body recombination and domain formation. *arXiv:1308.1961* (2013).

[34] Lipparini, E., Stringari, S Sum Rules and Giant Resonances. *Phys. Rep.* **175**, 103 (1989).

[35] Nozieres, P., & Pines, D. The theory of quantum liquids. *Perseus Ed., Cambridge, MA* (1999).

[36] Chin, C. & Julienne, P. S. Radio-frequency transitions on weakly bound ultracold molecules. *Phys. Rev. A* **71**, 012713 (2005).

[37] Massignan, P. & Bruun, G. M. Repulsive polarons and itinerant ferromagnetism in strongly polarized Fermi gases. *Eur. Phys. J D* **65**, 83–89 (2011).

[38] Taylor, E., Zhang, E., Schneider, W.& Randeria, M. Colliding clouds of strongly interacting spin-polarized fermions. *Phys. Rev. A* **84**, 063622 (2013).

[39] Sanner, C., Su, E., Keshet, A. , Huang, W., Gillen, J., Gommers, R.,& Ketterle, W. Speckle Imaging of Spin Fluctuations in a Strongly Interacting Fermi Gas. *Phys. Rev. Lett.* **106**, 010402 (2011).

[40] Nascimbene, S., Navon, N., Pilati, S. , Chevy, F., Giorgini, S., Georges, A.,& Salomon, C. Fermi-Liquid Behavior of the Normal Phase of a Strongly Interacting Gas of Cold Atoms. *Phys. Rev. Lett.* **106**, 215303 (2011).

[41] Kashimura, T., Watanabe, R., & Ohashi, Y. Spin susceptibility and fluctuation corrections in the BCS-BEC crossover regime of an ultracold Fermi gas. *Phys. Rev. A* **86**, 043622 (2012).

[42] Koschorreck, M., Pertot, D., Vogt, E., Frohlich, B., Feld, M. & Kohl, M. Attractive and repulsive Fermi polarons in two dimensions. *Nature* **485**, 619 (2012).

[43] Haller, E., Gustavsson, M., Mark, M. J., Danzl, J. G., Hart, R., Pupillo, G. & Nägerl, H.-C. Realization of an excited, strongly correlated quantum gas phase. *Science* **325**, 1224–1227 (2009).

[44] Vichi, L., & Stringari, S. Collective oscillations of an interacting trapped Fermi gas. *Phys. Rev. A* **60**, 474 (1999).

[45] Jeon, J. W., & Mullin, W. J. Theory of spin diffusion of dilute, polarized fermions for all temperatures. *J. Low Temp. Phys.* **67**, 421 (1987).

[46] Bruun, G. Spin diffusion in Fermi gases. *New J. Phys.* **13**, 035005 (2011).

[47] Enss, T. Transverse spin diffusion in strongly interacting Fermi gases. *Phys. Rev. A* **88**, 033630 (2013).

[48] Bruun, G., Recati, A., Pethick, C. J.., Smith, H.& Stringari, S. Collisional properties of a polarized Fermi gas with resonant interactions. *Phys. Rev. Lett* **100**, 240406 (2011).

[49] Bishop, R. F., Ghassib, H. B.& Strayer, M. R. Composite pairs and effective two-body scattering in a many-body medium. *Phys. Rev. A* **13**, 1570 (1976).

[50] Bruun, G. M., & Smith, H. Viscosity and thermal relaxation for a resonantly interacting Fermi gas. *Phys. Rev. A* **72**, 043605 (2005).

[51] Enss, T. Quantum critical transport in the unitary Fermi gas. *Phys. Rev. A* **86**, 013616 (2012).

[52] Bluhm, M., & Schäfer, T. Medium effects and the shear viscosity of the dilute Fermi gas away from the conformal limit. *Phys. Rev. A* **90**, 063615 (2014).